Modeling analysis of the effect of iron enrichment on dimethyl sulfide dynamics in the NE Pacific (SERIES experiment)

Yvonnick Le Clainche,[1] Maurice Levasseur,[1] Alain Vézina,[2] René-Christian Bouillon,[3] Anissa Merzouk,[1] Sonia Michaud,[4] Michael Scarratt,[4] Chi Shing Wong,[5] Richard B. Rivkin,[6] Philip W. Boyd,[7] Paul J. Harrison,[8] William L. Miller,[9] Cliff S. Law,[10] and François J. Saucier[11]

Received 7 March 2005; revised 27 September 2005; accepted 20 October 2005; published 21 January 2006.

[1] The large-scale iron enrichment conducted in the NE Pacific during the Subarctic Ecosystem Response to Iron Enrichment Study (SERIES) triggered a phytoplankton bloom dominated successively by nanophytoplankton and large diatoms. During the first 14 days, surface dimethyl sulfide (DMS) levels increased both inside (up to 22 nmol L^{-1}) and outside (up to 19 nmol L^{-1}) the patch, with no consistent Fe effect. Later, DMS concentrations became sixfold lower inside the patch than outside. In this study, we used a DMS budget module embedded in a one-dimensional ocean turbulence model to investigate the contribution of the interacting physical, photochemical, and biological processes to this particular DMS response. Temporal variations in biological net DMS production were reconstructed using an inverse modeling approach. Our results show that short-term (days) variations in both the physical processes (i.e., turbulent mixing and ventilation) and the biological cycling of DMS are needed to explain the time evolution of DMS concentrations both outside and inside the Fe-enriched patch. The biological net DMS production was generally high (up to 0.35 nmol L^{-1} h^{-1}) and comparable outside and inside the patch during the first 10 days, corresponding to the observed accumulation of DMS inside and outside the patch. Later, it became negative (net DMS biological consumption) inside the patch, suggesting a change in dimethylsulfoniopropionate bacterial metabolism. This study stresses the importance of short-term variations in biological processes and their sensitivity to the physical environment in shaping the DMS response to iron enrichment.

Citation: Le Clainche, Y., et al. (2006), Modeling analysis of the effect of iron enrichment on dimethyl sulfide dynamics in the NE Pacific (SERIES experiment), *J. Geophys. Res.*, *111*, C01011, doi:10.1029/2005JC002947.

1. Introduction

[2] High-nutrient low-chlorophyll (HNLC) waters covered about 30% of the world ocean [*Baliño et al.*, 2001]. *Martin and Fitzwater* [1988] first suggested that low iron (Fe) concentration in these waters was limiting phytoplankton growth and preventing the complete utilization of macronutrients. HNLC waters are found in the eastern equatorial Pacific, the ice-free Southern Ocean, and the subarctic North Pacific [*Chisholm and Morel*, 1991]. Results from the 8 first large-scale Fe enrichment experiments conduced so far have clearly shown that variations in Fe delivery to these HNLC waters may significantly influence the carbon cycle, CO_2 air-sea exchanges, and ultimately climate [*de Baar et al.*, 2005]. Variations in Fe deposition to HNLC waters may also affect the oceanic production of other climatically active gases such as dimethyl sulfide (DMS) [*Watson and Liss*, 1998, *Lawrence*, 2002].

[1]Département de Biologie (Québec-Océan), Université Laval, Quebec, Quebec, Canada.
[2]Bedford Institute of Oceanography, Fisheries and Oceans Canada, Dartmouth, Nova Scotia, Canada.
[3]Department of Chemistry and Biochemistry, University of North Carolina at Wilmington, Wilmington, North Carolina, USA.
[4]Maurice Lamontagne Institute, Fisheries and Oceans Canada, Mont-Joli, Quebec, Canada.
[5]Institute of Ocean Sciences, Fisheries and Oceans Canada, Sidney, British Columbia, Canada.
[6]Ocean Sciences Centre, Memorial University of Newfoundland, St. John's, Newfoundland, Canada.
[7]Centre for Chemical and Physical Oceanography, National Institute for Water and Atmospheric Research and Department of Chemistry, University of Otago, Dunedin, New Zealand.
[8]Atmospheric, Marine and Coastal Environment Program, Hong Kong University of Science and Technology, Hong Kong, China.
[9]Department of Marine Sciences, University of Georgia, Athens, Georgia, USA.
[10]National Institute of Water and Atmospheric Research, Wellington, New Zealand.
[11]Institut des Sciences de la Mer de Rimouski, Université du Québec à Rimouski, Rimouski, Quebec, Canada.

0148-0227/06/2005JC002947

[3] The DMS is the main volatile organic sulfur compound produced naturally in the ocean by the marine ecosystem [*Malin and Kirst*, 1997]. It results from the enzymatic cleavage of its precursor dimethylsulfoniopropionate (DMSP), a compound produced to varying degrees by many phytoplankton species [*Keller*, 1989; *Liss et al.*, 1994] and released into the water through exudation, cell lysis and grazing [*Kiene et al.*, 1996]. Oceanic DMS is lost through bacterial consumption [*Kiene and Bates*, 1990], photodegradation by UV radiation [*Toole et al.*, 2003] and ventilation to the atmosphere [*Barnard et al.*, 1982]. The ventilation of DMS is the largest natural source of atmospheric sulfur [*Bates et al.*, 1992]. Once in the atmosphere, DMS is oxidized to form non–sea salt sulfate and methanesulfonate (MSA) aerosols [*Andreae and Crutzen*, 1997]. These sulfate particles may alter the radiation budget of the Earth through modifications of cloud optical properties, especially by forming cloud condensation nuclei (CCN) that increase the cloud albedo [*Clarke et al.*, 1998] and consequently exert a cooling effect on our climate [*Charlson et al.*, 1987].

[4] Large-scale iron enrichment experiments conducted in the Equatorial Pacific (IronEx II) and in the Southern Ocean (SOIREE and EisenEx) consistently resulted in an increase in DMS concentrations in the Fe-enriched patch, while the DMS concentrations remained very low and stable in untreated waters [*Turner et al.*, 1996, 2004]. Results from modeling studies also suggest that DMS production may increase in HNLC regions as a result of climate changes. In a simulation of $2 \times CO_2$ climate, *Bopp et al.* [2003] predicted that the largest increases of surface DMS concentration would occur in the HNLC regions, especially in the Southern Ocean. The modeling study of *Gabric et al.* [2003] simulated an increase in DMS production in the Eastern Antarctic Southern Ocean under a $3 \times CO_2$ climate. Although neither of these two modeling studies took into account the iron limitation of phytoplankton production, they highlight the potential sensitivity of HNLC waters in terms of DMS production, and the need for a better understanding of the biological cycling of DMS in Fe-limited waters.

[5] In July–August 2002, a large-scale iron enrichment experiment was conducted for the first time in the Northeastern Pacific Ocean (Subarctic Ecosystem Response to Iron Enrichment Study (SERIES)). The iron enrichment triggered a phytoplankton bloom dominated successively by DMSP-rich nanophytoplanktons and large diatoms [*Boyd et al.*, 2004]. The nanophytoplankton bloom rapidly declined 10 days after the fertilization presumably because of an increase in microzooplankton grazing. The DMSP concentration mainly followed the nanophytoplankton abundance, first doubling its initial level before decreasing to background values on day 12 of the experiment. The impact of the iron enrichment on DMS concentrations was novel and unexpected. During the first 14 days of the experiment, DMS concentrations increased to similar levels both inside and outside the Fe-enriched patch, suggesting little if any influence of the Fe-induced nanophytoplankton bloom on DMS production inside the patch. In addition, DMS concentrations became consistently lower inside the patch than outside during the end of the experiment.

[6] In this study, a DMS budget module embedded in a one-dimensional (1-D) ocean turbulence model was used to investigate the contribution of the interacting physical, photochemical, and biological processes to the dynamics of the surface ocean DMS pool during SERIES, both inside and outside the Fe-enriched patch. Temporal variations in biological net DMS production inside and outside the patch were reconstructed using an inverse modeling approach. Our main objective was to understand the natural variability of DMS observed in the untreated waters as well as the unusual DMS response to iron enrichment during SERIES. The paper is organized as follows: SERIES is first briefly introduced in section 2, with a principal focus on the DMSP and DMS observations; the model and its applications are described in section 3, modeling results are presented in section 4, discussed in section 5, and summarized in section 6.

2. SERIES Experiment

[7] The Subarctic Ecosystem Response to Iron Enrichment Study (SERIES) was conducted in the Northeastern Pacific Ocean between 9 July and 4 August 2002, with DMS(P) measurements ending on 28 July (sampling day 19). A 77 km^2 patch of surface water centered at 50°12′N; 144°45′W near Ocean Station Papa was enriched with dissolved Fe and the conservative tracer sulfur hexafluoride (SF_6) on 9 July. A second infusion of iron was conducted on 17 July following a rapid deepening of the surface mixed layer [*Boyd et al.*, 2004]. Seawater samples for DMSP and DMS measurements were collected using a rosette/CTD system equipped with 10 L Niskin bottles on board of the two ships *B/O El Puma* and *CCGS John P. Tully.* The "in patch" samples were collected at the center of the Fe-enriched patch (determined from the SF_6 distribution), whereas most of the "out patch" samples were collected northeast of the patch away from its anticipated drift. Aboard *B/O El Puma*, samples were collected at 6 depths on the basis of irradiance profiles (100, 33, 10, 3.3, 1 and 0.15% of surface incident light) and DMSP and DMS were analyzed according to the method described by *Scarratt et al.* [2002]. These samples were also used for chlorophyll *a* (Chl *a*) determination (all depths) and phytoplankton identification and enumeration (100% of surface incident light). Aboard *CCGS John P. Tully*, samples were collected up to 24 July (sampling day 15) at 5 to 8 depths (5, 10, 20, 35, 45, 55, 75, 100 m) and only DMS measurements were performed following the method described by *Wong et al.* [2005]. An intercalibration study conducted at sea between the two ships showed that the two sets of DMS measurements were compatible and could be combined for further analysis (M. Levasseur et al., DMSP and DMS dynamics during a mesoscale iron fertilization experiment in the Northeast Pacific. part I. Temporal and vertical distributions, submitted to *Deep-Sea Research*, *Part II*, 2005). In this study, the 18 daily (except day 16) "in patch" DMSP and DMS data used came exclusively from the *B/O El Puma*, while the 12 "out patch" DMS data combined the data from the two ships. DMSP concentrations were only measured 5 times outside the Fe-enriched patch by the *B/O El Puma*.

2.1. Variations in Surface Chlorophyll *a*, DMSP, and DMS Concentrations

[8] The iron enrichment resulted in a phytoplankton bloom dominated successively by nanophytoplankton from

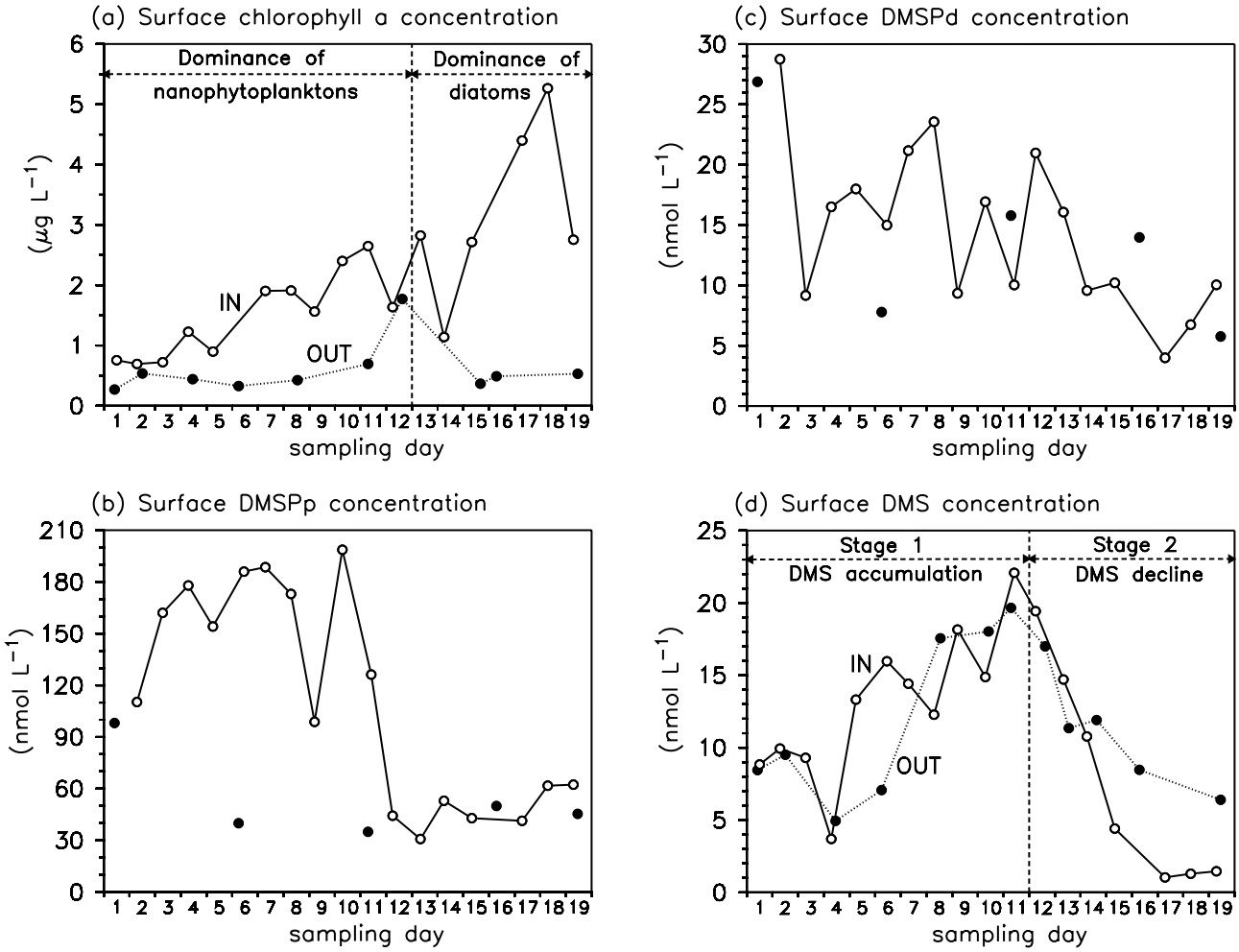

Figure 1. Time evolution of surface concentrations observed during SERIES inside (open circles and solid line) and outside (solid circles and optional dotted line) the Fe-enriched patch of (a) chlorophyll *a* (μg L^{-1}), (b) particulate DMSP (DMSPp, nmol L^{-1}), (c) dissolved DMSP (DMSPd, nmol L^{-1}), and (d) DMS (nmol L^{-1}). Note that these surface concentrations represent well the average over the surface mixed layer.

day 1 to day 12 (numerically dominated by prymnesiophytes, notably *Emiliania huxleyi*) and large diatoms after day 12 (pennates and centric diatoms) [*Boyd et al.*, 2004; A. Marchetti et al., Phytoplankton processes I: Changes in biomass and community composition due to mesoscale iron enrichment in the NE subarctic Pacific, submitted to *Deep-Sea Research, Part II*, 2005]. This bloom was characterized by a sixfold increase in chlorophyll *a* inside the Fe-enriched patch, while there was no notable change in phytoplankton abundance in the untreated waters (Figure 1a). Temporal variations in particulate DMSP concentrations (DMSPp) inside the Fe-enriched patch followed closely the iron induced nanophytoplankton bloom (Figure 1b), increasing from ~100 nmol L^{-1} at the onset of the experiment to ~170 nmol L^{-1} during days 4–10 and then declining abruptly between days 10 and 12 to levels of ~40 nmol L^{-1} similar to those observed outside the patch. The distribution of dissolved DMSP (DMSPd) concentrations inside and outside the patch was more variable, with no consistent increase inside the Fe-enriched patch (Figure 1c).

[9] Variations in DMS concentrations during SERIES (Figure 1d) considerably contrasted with those reported from previous large-scale iron enrichment experiments [*Turner et al.*, 1996, 2004] in three major ways. First, DMS concentrations in the untreated surrounding waters were elevated at the onset of the experiment and further increased up to ~19 nmol L^{-1} during the following 11 days. The average surface DMS concentration of ~12 nmol L^{-1} over the 19 days sampling period was four times higher than the mean for the global open ocean [*Kettle et al.*, 1999]. The Northeast Pacific subarctic gyre province is known to be DMS-rich in summer [*Kettle and Andreae*, 2000; *Wong et al.*, 2005]. This richness was empirically attributed to the abundance of DMSP-rich prymnesiophytes in the region [*Wong et al.*, 2005]. However, there were no obvious sources for the observed short-term variability in surface DMS outside the patch. The increase in DMS concentrations outside the patch was not paralleled by an increase in DMSP concentrations, suggesting that the accumulation of DMS was rather resulting from a change in physical forcing or a change in DMSP metabolisms

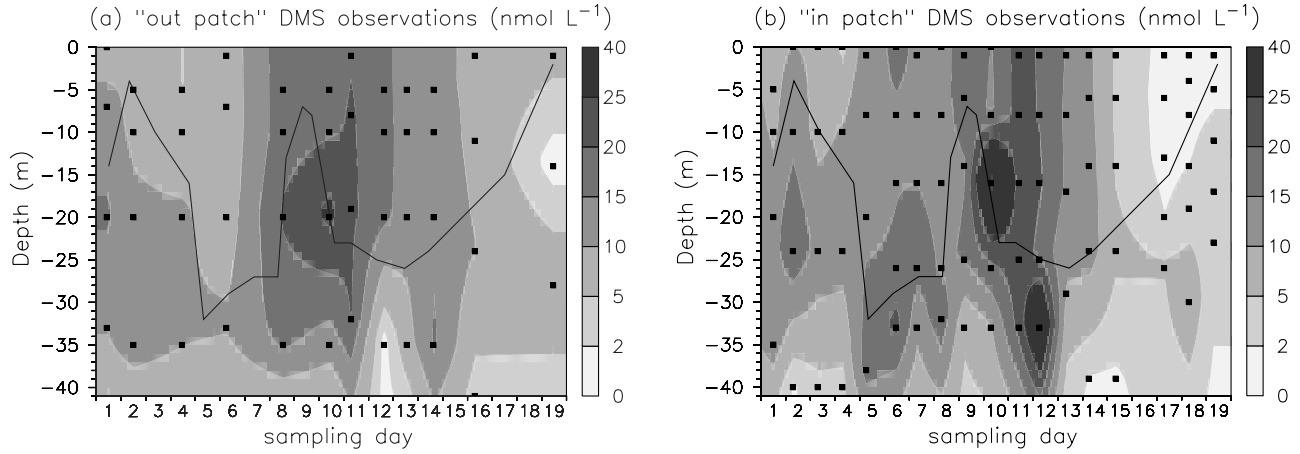

Figure 2. Time evolution of DMS concentrations (nmol L^{-1}) in the upper 40 m ocean interpolated from the SERIES observations (a) outside and (b) inside the Fe-enriched patch. The solid line depicts the time evolution of the reference surface mixed layer depth (m) diagnosed from the in situ observed density profiles. The squares superimposed on the plots indicate exactly the positions of the DMS in situ measurements from SERIES.

than a change in DMSP pool size. Second, the general distribution of DMS inside the Fe-enriched patch was remarkably similar to the one outside the patch during the first 14 days of the experiment, making the effect of iron more difficult to assess only on the basis of the DMS observations. Like outside the patch, the surface DMS concentrations inside the patch increased from initial conditions ($\sim$9 nmol L^{-1}) to a maximum on day 11 ($\sim$22 nmol L^{-1}), before decreasing by day 19. The sampling period was thus characterized by two stages identifiable both inside and outside the Fe-enriched patch: a DMS accumulation stage from day 1 to day 11 (stage 1) and a DMS reduction stage from day 12 to day 19 (stage 2). Third, the DMS concentrations decreased more intensely inside the patch than outside during stage 2 and became consistently lower inside the patch than outside after day 14, most probably reflecting a change in DMSP metabolism related to the iron-induced diatom bloom.

2.2. Vertical Distributions of DMS During SERIES

[10] Figure 2 shows the time evolution of DMS concentrations in the upper 40 m ocean inside and outside the Fe-enriched patch. The similitude between the distribution of DMS inside and outside the patch is also reflected in the vertical distributions. The DMS concentrations were homogeneous over the upper ocean mixed layer, indicating that surface concentrations were representative of the mixed layer DMS pool. The highest DMS concentrations were measured in the subsurface layer around 15–20 m on day 10, both inside and outside the patch. Below 30 m (mean depth of the seasonal pycnocline), the variability in DMS concentrations, especially inside the patch, was related to the fluctuations of the seasonal pycnocline present in the observations (Figure 3a). A local DMS maximum $\sim$37 nmol L^{-1} was measured inside the patch on day 12 at 33 m, in the subpycnocline waters. This maximum was associated with very large concentrations of DMSP and probably resulted from the presence of *Phaeocystis* spp. colonies. Otherwise, *Phaeocystis* spp. abundance remained below 60,000 cells L^{-1} both inside and outside the patch in surface waters.

3. Description of the Model

[11] DMS concentrations in the mixed layer are controlled by interacting physical (turbulent diffusion, ventilation), photochemical (photodegradation), and biological (biological production and bacterial consumption) processes [*Simó*, 2004]. Especially in a short-timescale study like SERIES, the relative contributions of these mechanisms can only be resolved using a model considering both physical and biogeochemical processes. In this study, our modeling work evolved in three steps. First, the 1-D numerical model of the ocean water column General Ocean Turbulence Model (GOTM) was used to compute the turbulent vertical mixing. Second, a DMS budget module (Figure 4) was embedded in the physical upper ocean model. Finally, we used an inverse modeling approach based on the observed vertical distributions of DMS to reconstruct the variations in biological net DMS production outside and inside the Fe-enriched patch. These steps are detailed in the three following subsections.

3.1. Physical Ocean Model

[12] The turbulent vertical mixing was computed by GOTM according to a two-equation k-ε turbulence closure scheme [*Burchard et al.*, 1999] (see also http://www.gotm.net). The turbulent kinetic energy (TKE) k and the dissipation rate ε are calculated via prognostic equations, which consider turbulence generation by wind, buoyancy and shear production, as well as dissipation and turbulent diffusion. This model has already been successfully coupled with a biogeochemical model to simulate the seasonal evolution of the DMS(P) pools in the Sargasso Sea [*Le Clainche et al.*, 2004] and in the North Sea [*Archer et al.*, 2004].

[13] The same eddy diffusivity was attributed to all tracers (temperature, salinity, DMS) on the basis of the assumption of fully developed turbulence [*Burchard et al.*,

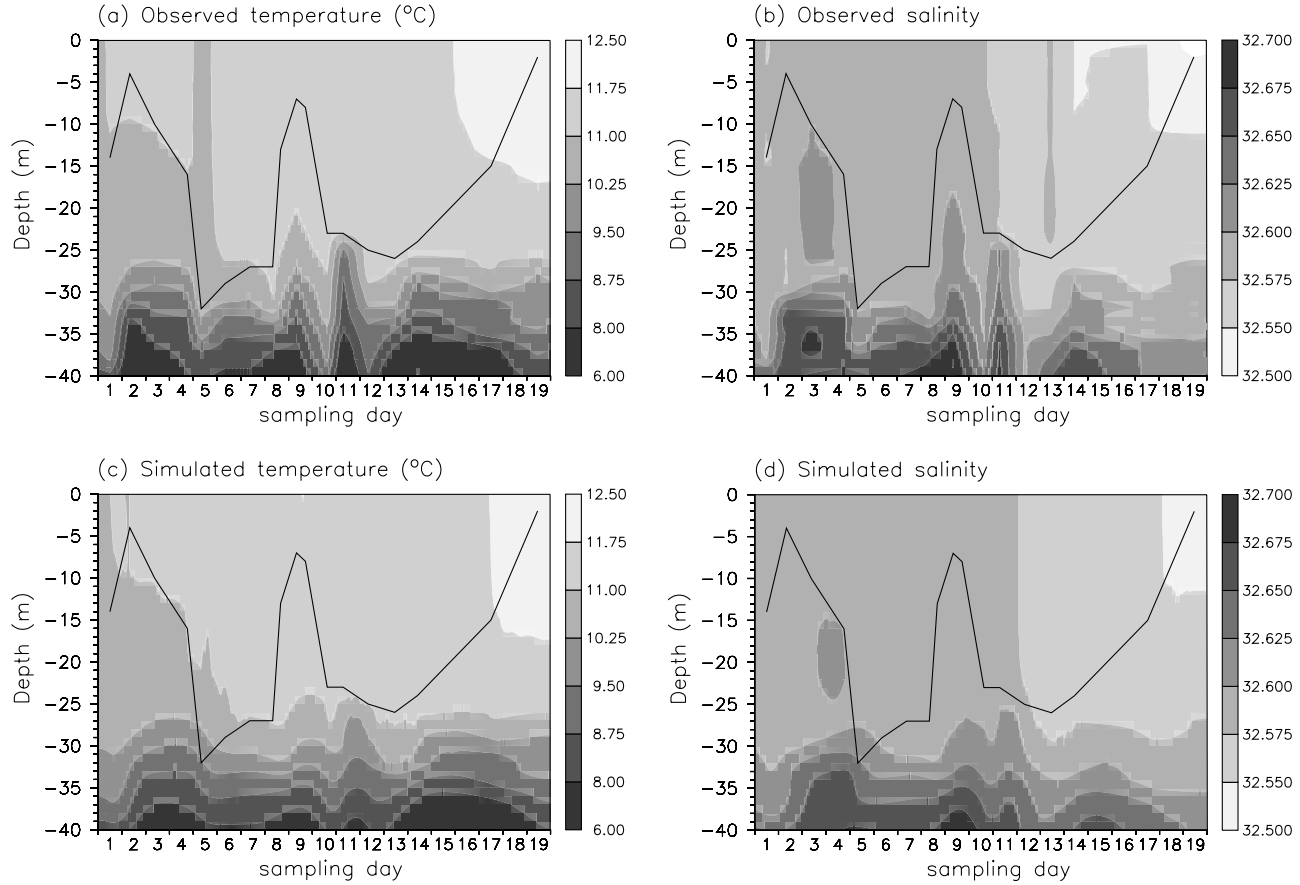

Figure 3. Time evolution in the upper 40 m of oceanic (a) temperature (°C) and (b) salinity interpolated from the SERIES observations inside the Fe-enriched patch and (c) temperature (°C) and (d) salinity simulated by the model using a 24 h relaxation toward the T/S observations from inside the patch. The solid line depicts the time evolution of the reference surface turbulent mixed layer depth (m) diagnosed from the in situ observed density profiles.

1999]. The stability function was calculated following the method of *Kantha and Clayson* [1994]. We used the parameterizations derived from *Large et al.* [1994] to promote increased mixing induced by shear instability and internal wave activity under stratified conditions [*Kantha and Clayson*, 1994]. On the basis of *Cummins and Lagerloef* [2002], we used a constant monthly mean value for July 2002 of 0.765 m day^{-1} for Ekman pumping.

[14] The model used a regular vertical resolution with 100 layers of 1 m thickness from the surface to 100 m depth and an integration time step of 5 min. Initialized with temperature and salinity profiles observed on 9 July 2002, it was forced with the wind speed (Figure 5b) calculated from the postprocessed onboard wind measurements during SERIES. The solar and nonsolar components of the surface heat flux were computed through the bulk formula implemented in GOTM. The nonsolar heat flux is a function of hourly averaged meteorological data collected on board (air temperature, surface air pressure, air relative humidity) or interpolated (cloud fraction) from daily NCEP-CDAS reanalysis [*Kalnay et al.*, 1996].

[15] The sea surface salinity (SSS) and the sea surface temperature (SST) were restored every day with the in situ measurements from the *CCGS John P. Tully*. The SSS relaxation replaces the effect of the surface freshwater

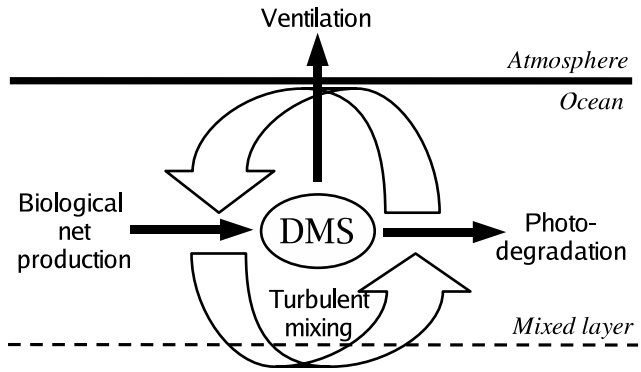

Figure 4. Conceptual scheme of the DMS budget module. The biological net DMS production corresponds to the DMS gross production by both bacterial and algal conversion of DMSP to DMS minus the bacterial DMS consumption. The DMS is lost through photodegradation and ventilation to the atmosphere. The DMS pool is also affected by turbulent vertical mixing, which determines its vertical distribution.

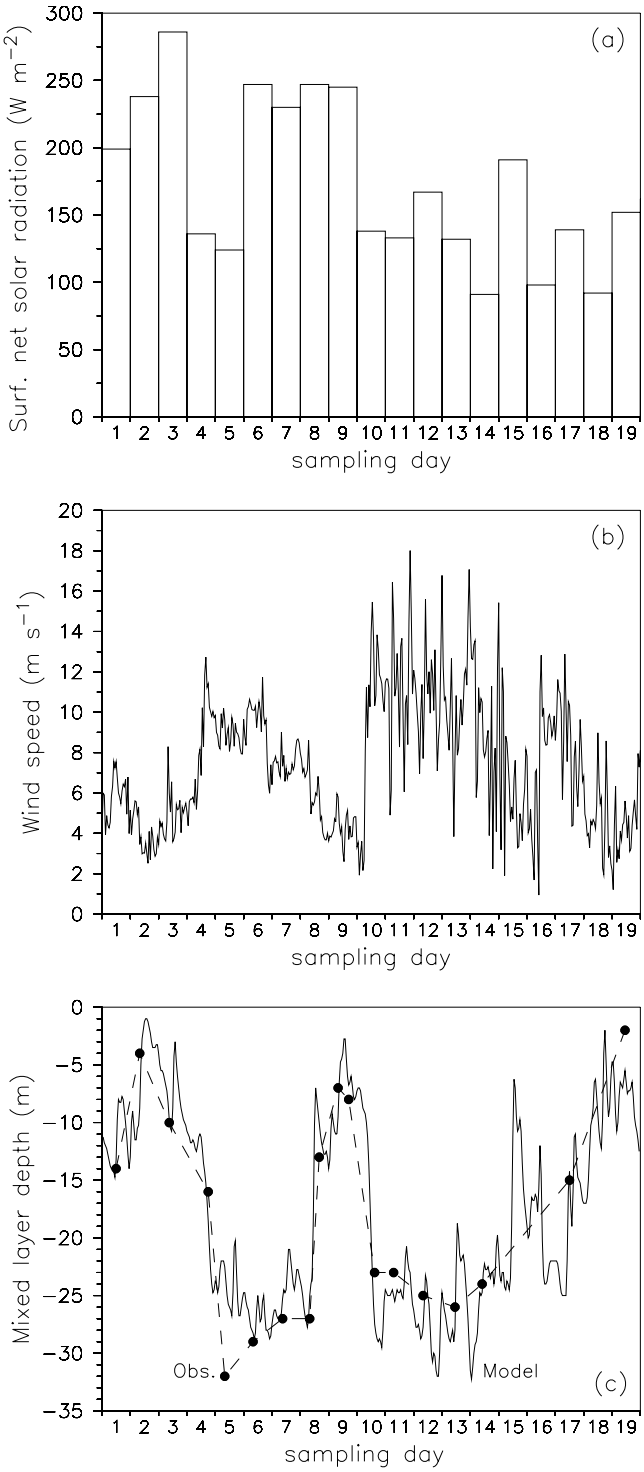

Figure 5. Time evolution of (a) daily surface net solar radiation (W m^{-2}) from NCEP/NCAR reanalysis, (b) hourly average of measured wind speed (m s^{-1}), and (c) turbulent mixed layer depth simulated by GOTM (solid line) and reference surface mixed layer depth diagnosed from the in situ observed density profiles inside the Fe-enriched patch (dashed line and solid circles).

flux, while the SST relaxation acts as a flux correction on the surface net heat flux calculated by GOTM. The temperature (T) and salinity (S) profiles were also restored over the whole vertical domain (0–100 m) with the same relaxation time constant of 24 h and with the temperature and salinity (hereinafter T/S) observations linearly interpolated by GOTM over time and depths (to the 1 m vertical resolution). We used only the T/S observations from the "in patch" stations located at the Fe-enriched patch center (determined from the SF_6 distribution), since they offer the best daily coverage of measurements to restore the model. Furthermore, we also ran a simulation by using the T/S observations from the "out patch" stations, but the differences were not sufficient to justify a distinction in the physical forcing between inside and outside the patch (see also part 4.3 on sensitivity tests). The use of the same physical forcing (same wind forcing and T/S restoring) to run the model inside and outside the patch made the comparison between "in patch" and "out patch" simulations easier to interpret, especially for the budget in the mixed layer.

3.2. DMS Budget Module

[16] The DMS budget module only includes biological net DMS production and DMS lost through photodegradation and ventilation to the atmosphere (Figure 4). The biological net DMS production corresponds to the gross DMS production by both bacterial and algal conversion of DMSP to DMS minus the bacterial DMS consumption. We chose to combine all biological processes into one net flow, which is in a way equivalent to a Net Community Production (NCP) of DMS, for two major reasons. First, we do not have sufficient observations on the different biological processes to reconstruct them independently. Second, we do not have the mechanistic understanding of DMS production and loss processes that would allow us to simulate their short-term variability. For example, current process models of DMS dynamics assume linear rates of production and consumption that are linked through changes in pool sizes [*Vézina*, 2004]. However, we know that production and consumption rates are highly variable and uncoupled [*Kiene and Bates*, 1990]. Therefore we strongly suspect that linear models, possibly adequate for reproducing large-scale and annual patterns, will not work at these short timescales. Furthermore, the reconstructed biological net DMS production rates can be related to other variables observed during the experiment, allowing us to investigate interactions and infer the processes acting at these short timescales.

[17] The DMS budget module was coupled with GOTM using the same numerical method than for the coupling between our more complex DMS cycle model and GOTM [*Le Clainche et al.*, 2004]. The DMS tracer was introduced in GOTM using the following equation:

$$\frac{\partial DMS}{\partial t} = [DMS]_{netprod} - [DMS]_{photo} - [DMS]_{ventil}^{z=o} + \frac{\partial}{\partial z}\left[\nu_t \frac{\partial DMS}{\partial z} + DMS \cdot w\right] + \delta \cdot \Delta_{DMS} \quad (1)$$

where

$[DMS]_{netprod}$ biological net DMS production as defined above.

$[DMS]_{photo}$ DMS photodegradation;
$[DMS]^{z=o}_{ventil}$ DMS ventilation to the atmosphere calculated only at the surface level (z = 0);
$\nu_t \frac{\partial DMS}{\partial z}$ turbulent flux of DMS with the eddy diffusivity ν_t calculated by GOTM;
w mean vertical velocity related to the Ekman pumping;
$\delta \cdot \Delta_{DMS}$ effect of patch dilution on the "in patch" DMS concentration;

[18] The additional supply/loss DMS term representing the effect of patch dilution due to the lateral entrainment of the surrounding waters was only taken into account in the simulation of DMS inside the patch. It was calculated as the product of the estimated strain rate δ of the SF_6-labeled patch [*Boyd et al.*, 2004] and the "In-Out" DMS concentration gradient Δ_{DMS}.

[19] The sea-to-air flux of DMS was controlled by the transfer velocity k_w calculated following *Nightingale et al.* [2000] and the ocean surface DMS concentration: $F_{DMS} = k_w\ DMS_{z=0}$ with $k_w = (0.222 \times ws^2 + 0.333 \times ws).\ (\frac{600}{Sc})^{1/2}$ where ws is the wind speed and Sc the Schmidt number for DMS calculated following the formula given by *Saltzman et al.* [1993].

[20] The photodegradation term was applied during daylight, that is, from sunrise (0400 local time) to sunset (2000 local time), following a sinusoidal function (maximum at local noon) based on the daily DMS photodegradation rates. The DMS photodegradation rate profiles were calculated using the apparent quantum yield (AQY) values for DMS photodegradation together with in situ DMS concentrations, modeled solar irradiance and measured seawater optical properties following the work of R.-C. Bouillon et al. (The effect of mesoscale iron enrichment on the marine photochemistry of dimethylsulfide in the NE subarctic Pacific, submitted to *Deep-Sea Research, Part II*, 2005). We used either the measured AQY values or the estimated AQY values from the relationship between AQY and NO_3^- concentration presented by *Bouillon and Miller* [2004]. The photodegradation rates differed inside the patch from outside the patch according to the changes in both DMS and NO_3^- concentrations resulting from the iron-induced phytoplankton bloom [*Bouillon and Miller*, 2004]. Moreover, the rates decreased rapidly with depth following the attenuation of UV radiation.

[21] Since the DMS photodegradation, the surface DMS ventilation and the physical effects (vertical turbulent mixing and advection, plus the lateral dilution effect inside the patch) were calculated by the coupled model, the only unknown flow in the DMS budget (equation (1)) was the biological net DMS production (see Figure 4).

3.3. Reconstruction of Biological Net DMS Production

[22] From the vertical distributions of DMS measured in situ during SERIES, we used an inverse modeling approach to reconstruct the biological net DMS production required to reproduce the observed DMS pools inside and outside the patch. We assumed that all the variations not represented by the physical and photochemical processes can be attributed to biological processes. Despite its overall similarity with the approach used by *Toole and Siegel* [2004] to estimate bimonthly net biological community production of DMS from seasonal time series in the Sargasso Sea, our modeling work attempts to reconstruct short-term variations and differs mainly by the use of a 1-D physical ocean turbulence model to reproduce the rapid variations of the upper ocean mixed layer and their influence on the surface DMS pool.

[23] The biological net DMS production was calculated every simulated hour (inversion time step) for each vertical level as the difference between the DMS concentration estimated by the model (on the basis of photodegradation, ventilation and physical processes) and the DMS concentration interpolated from the observations:

$$[DMS]_{netprod} = \frac{\left([DMS]_{obs} - [DMS]_{estim}\right)}{\Delta t} \quad (2)$$

where $[DMS]_{obs}$ is the DMS concentration (nmol L^{-1}) linearly interpolated by GOTM both in time and over depth (to the 1 m vertical resolution) from the observations (in agreement with the measurements performed at 100 m depth, we fixed the DMS concentration to 0 nmol L^{-1} at the bottom of the model domain); $[DMS]_{estim}$ is the DMS concentration (nmol L^{-1}) estimated by resolving equation (1) without taking into account the net DMS production by the biological activity, and Δt is the 1 hour time step over which the biological net DMS production is computed.

[24] Once calculated, this hourly reconstructed biological net DMS production rate was used to update the DMS concentration at each vertical level in the model, before proceeding with the model integration.

[25] We know from inverse modeling theory that several possible solutions could exist depending on the approach taken to estimate the flow [*Parker*, 1994]. Even when reconstructing only one flow (ex. biological net DMS production) from one consistent data set of only one variable (ex. DMS concentration), we needed to make some assumptions to find a solution. Here, we assumed linear variations in time and in space (on the vertical) of DMS concentration between each daily DMS observation (sometimes less in the case of "out patch" data), as well as minimal variations in net DMS production between these observations. This implies that we did not consider any diel variations.

[26] We performed two simulations using this inverse method to reconstruct the changes of the biological net DMS production outside and inside the Fe-enriched patch during SERIES. The two simulations "out patch" and "in patch" differed by the set of DMS observations used for the reconstruction, the daily DMS photodegradation rates and the additional dilution effect for the "in patch" simulation. Both simulations started on 9 July 2002 at 1800 (local time is GMT minus 9h 40min) and ended on 29 July 2002 at 0000, covering the first 19 days of SERIES when DMS(P) observations were available. The first day of the SERIES experiment (sampling day 1) was 10 July 2002 and the outputs started from this date at 0000 in local time, since the spin-up of the 1-D turbulent ocean model occurred rapidly (on turbulent timescales).

[27] Given the homogenous distribution of DMS in the upper mixed layer (Figure 2), we assumed that the plankton and the associated DMS-related biological processes were also homogenously distributed in the mixed layer. Accordingly, the reconstructed biological net DMS productions

were vertically averaged over the surface turbulent mixed layer and smoothed over a 24 h Hanning window [*Press et al.*, 1986].

4. Model Results

4.1. Physical Environment As Simulated by GOTM

[28] The Turbulent Mixed Layer depth simulated by the model (hereafter named TML) was defined as the depth where the turbulent kinetic energy (TKE) decreased to less than 10^{-6} m^2 s^{-2}. This approach provides a dynamically based definition of the mixed layer variability, and allows a better visualization of the short-term mixing events generated by the model in relation to the high variability of the wind forcing (Figure 5b). The model reproduced adequately the variations of mixed layer depth observed during SERIES (Figure 5c). In agreement with the recommendations of *Brainerd and Gregg* [1995], the reference mixed layer depth was diagnosed as the first significant change (vertical gradient >0.01 kg m^{-3} m^{-1}) in the observed sigma-t profiles. We obtained nearly the same reference mixed layer depth (not shown) when diagnosed by applying a similar criterion (gradient >0.02°C m^{-1}) on the observed temperature profiles. By reproducing adequately the high variability of the mixing, we could capture its influence on the vertical distribution of DMS.

[29] The sampling period was characterized by a succession of deepening and shoaling of the TML (Figure 5c), mostly forced by variations in surface wind speed. Variations in surface net solar radiation (Figure 5a) were inversely related to wind speed during SERIES and thus strengthened the influence of the wind on the TML. A complete cycle of temporary shallow TML formation and destruction was recorded at midcruise. The rapid development of this shallow mixed layer (TML depth < 10 m) occurred during days 8–9, after a period of stability of the TML. This shoaling event ended abruptly with the increase in wind speed (~10 m s^{-1} on average between days 10 to 15) causing the deepening of the TML down to the seasonal pycnocline.

[30] Given the use of a 24 h T/S relaxation time constant, the upper ocean temperature and salinity structures were well simulated by GOTM during SERIES (Figure 3). As noted above, the model reproduced a well-defined seasonal pycnocline at ~30 m. Although it also reproduced the vertical gradient in the 30–40 m zone, it did not completely capture the observed variations of the T/S characteristics. The localization of the patch near a front associated with the movement of the patch center can explain this variability. Indeed lateral horizontal T/S advection and diffusion along the pycnocline may have generated fluctuations, which involve rapid small variations in the different T/S observations at the patch center. Even with a 24 h T/S relaxation time constant, this feature cannot be reproduced by a 1-D ocean model. Nevertheless, the changes in vertical mixing above the seasonal pycnocline were well represented by GOTM, providing reliable physical support to this study.

4.2. Reconstructed Biological Net DMS Productions and DMS Budget in the Mixed Layer

[31] On the basis of the biological net DMS productions reconstructed inside and outside the Fe-enriched patch, we calculated the DMS budget in the mixed layer by considering the TML averaged contributions of the different processes (photochemical, physical and biological) involved in DMS dynamics (Figure 6).

[32] Our model results show that nonbiological processes (mixing, ventilation, and photodegradation) cannot totally explain the time evolution pattern (accumulation up to day 11 and subsequent decline to day 19) in DMS concentrations measured outside the Fe-enriched patch during SERIES (Figure 6). Despite the relative stability observed in the abundance and composition of the phytoplankton assemblage and in the size of the DMSP pool (Figure 1), the biological processes largely controlled the temporal variations in the DMS budget in the mixed layer outside the patch. The reconstructed biological net DMS production was generally around zero (no net production or loss) for most of the experiment, except for a period of high production between day 6 and day 10. This period of high biological net DMS production corresponds to the regime of DMS accumulation (days 4–11). Similarly, the decline in DMS concentration measured after day 11 was associated with a decrease in biological net DMS production to low rates and with high ventilation rates. These results clearly indicate that the natural variations in DMS concentrations measured in the untreated waters during SERIES resulted from a combination of biological and physical factors.

[33] Inside the Fe-enriched patch, the temporal variations in the DMS budget in the mixed layer were also largely controlled by biological net DMS production (Figures 6d and 6e). This importance of the biological processes inside the patch was more expected considering the iron-induced phytoplankton bloom and the associated large variations in the size of the DMSP pool (Figure 1). However, the levels of biological net DMS production reconstructed inside the patch were comparable with those reconstructed outside the patch, illustrating the complexity of the response of DMS production and consumption to iron enrichment during SERIES. The differentiation between the two DMS regimes (accumulation versus decline) was also obvious in the DMS budget inside the patch. The reconstructed biological net DMS production was positive but highly variable during stage 1 (days 1–11) and became negative during stage 2 (days 12–19) corresponding to a net DMS consumption by the microbial system (Figure 6d).

[34] In summary, the DMS budget in the upper mixed layer was largely determined by changes in biological net DMS production both inside and outside the patch during SERIES. Our inverse modeling reconstructions show that biological net DMS production was higher during stage 1 (days 1–11) of the experiment than during stage 2 (days 12–19). On average, stage 1 corresponded to a period of net DMS production (higher inside the patch than outside on average), whereas net DMS production was null (outside the patch) or even negative (inside the patch) during stage 2.

4.3. Sensitivity Test Inversions

[35] Models rely on basic assumptions and specific parameterizations that can moderately or profoundly affect their outputs. Before discussing in more details our results, we quantified the robustness of our model in reconstructing the biological net DMS production using a suite of sensi-

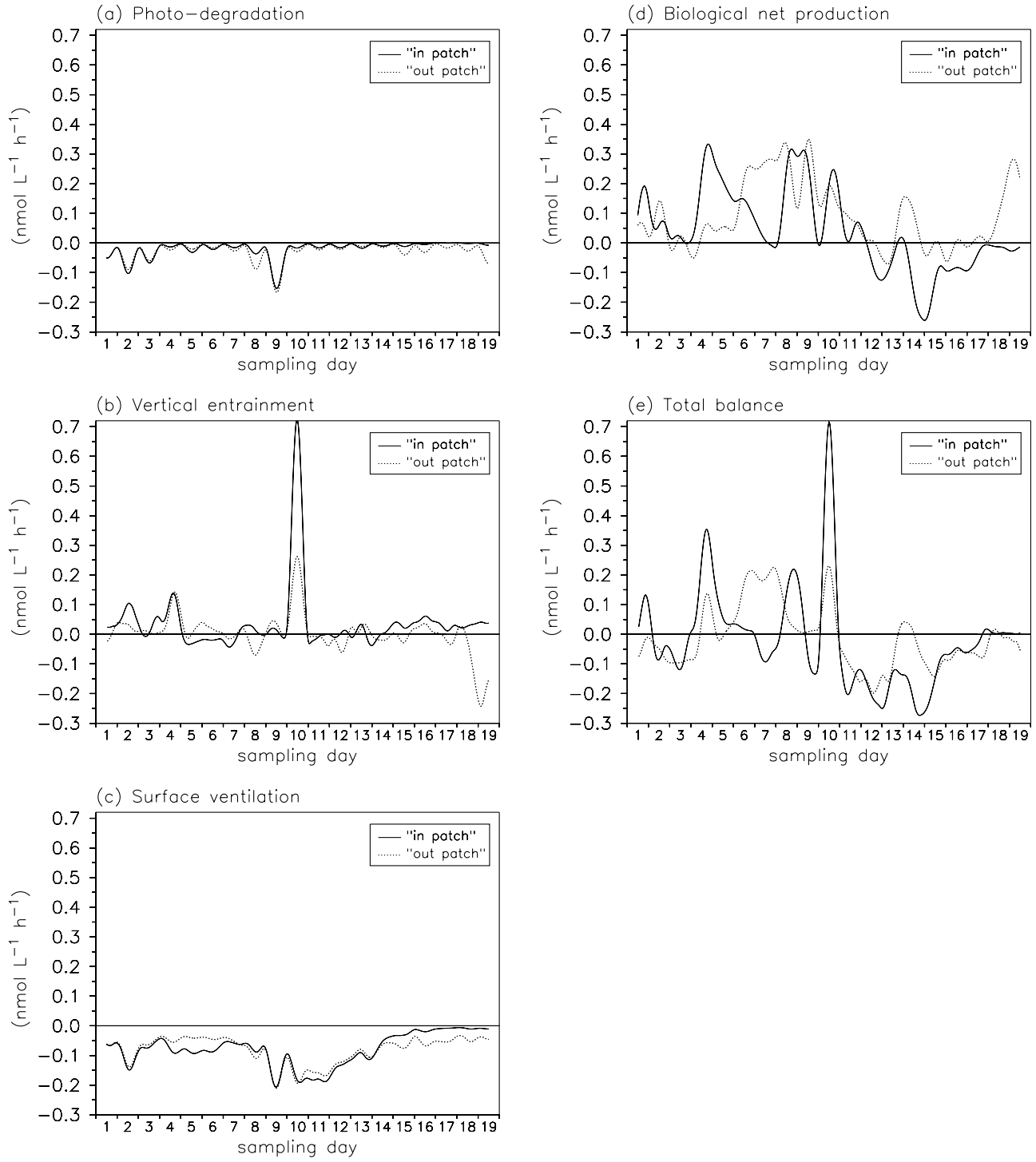

Figure 6. Time evolution (smoothed over a 24 h Hanning window) of the averaged contributions (nmol L^{-1} h^{-1}) of the different processes involved in DMS dynamics to the DMS budget in the TML: (a) DMS photodegradation, (b) DMS vertical entrainment, (c) surface DMS ventilation, (d) biological net DMS production, and (e) the total DMS balance in the TML (nmol L^{-1} h^{-1}) inside (solid line) and outside (dotted line) the Fe-enriched patch.

tivity test inversions (Table 1). Our objective was to determine if the reconstructed main patterns and the differences between inside and outside the patch were preserved when changing some technical aspects in the configuration of our model. We assessed the impact of these changes on the reconstructed biological net DMS production vertically averaged over the upper 30 m and time averaged over the two periods identified earlier: from sampling day 1 to day 11 (stage 1) and from sampling day 12 to day 19 (stage 2) (Table 1). The sensitivity was also evaluated by considering

Table 1. Reconstructed Biological Net DMS Production Vertically Averaged Over the Upper 30 m Ocean and Time Averaged Over the Two Stages and Surface DMS Flux Time Averaged Over the Whole Experiment in the Reference and the Sensitivity Inversions Outside and Inside the Fe Patch

	Reconstructed Biological Net DMS Production, nmol L^{-1} d^{-1} [a]								Surface DMS Flux, μmol m^{-2} h^{-1}			
	"Out Patch"				"In Patch"				"Out Patch"		"In Patch"	
	Day 1 to Day 11		Day 12 to Day 19		Day 1 to Day 11		Day 12 to Day 19		Day 1 to Day 19		Day 1 to Day 19	
	Mean	Percent	Mean	Percent	Mean	Percent	Mean	Percent	Mean	Percent	Mean	Percent
Reference Inversions												
Standard configuration	1.705		−0.443		2.347		−1.774		1.203		1.264	
Sensitivity Inversions[b]												
Model integration time step of 15 min	1.709	+0.2	−0.431	−2.7	2.333	−0.6	−1.773	−0.1	1.210	+0.6	1.257	−0.6
Inversion time step of 5 min	1.712	+0.4	−0.421	−5.0	2.379	+1.4	−1.777	+0.2	1.221	+1.5	1.280	+1.3
Inversion time step of 3 hours	1.696	−0.5	−0.450	+1.6	2.282	−2.8	−1.726	−2.7	1.194	−0.7	1.253	−0.9
Mellor-Yamada turbulence scheme	1.691	−0.8	−0.459	+3.6	2.287	−2.6	−1.774	0.0	1.197	−0.5	1.224	−3.2
T/S relaxation at 6 hours	1.709	+0.2	−0.420	−5.2	2.356	+0.4	−1.804	+1.7	1.206	+0.2	1.269	+0.4
T/S relaxation at 5 days (in the mass)	1.707	+0.1	−0.443	0.0	2.345	−0.1	−1.772	−0.1	1.205	+0.2	1.264	0.0
T/S differentiation between "in" and "out"	1.717	+0.7	−0.430	−2.9					1.204	+0.1		
No dilution effect for "in patch"					2.205	−6.1	−1.439	−18.9			1.265	+0.1
DMS flux parameterization [*Liss and Merlivat*, 1986]	1.431	−16.1	−0.734	+65.7	2.024	−13.8	−2.007	+13.1	0.852	−29.2	0.907	−28.2
DMS flux parameterization [*Wanninkhof*, 1992]	1.920	+12.6	−0.180	−59.4	2.612	+11.3	−1.546	−12.9	1.498	+24.5	1.577	+24.8
No DMS photodegradation	1.410	−17.3	−0.630	+41.3	2.133	−9.1	−1.851	+4.3	1.205	+0.2	1.267	+0.2

[a]Vertically averaged over the upper 30 m ocean.
[b]For the sensitivity inversions, the changes from the reference inversions are also indicated as relative percentage.

the change in the surface DMS flux time averaged over the whole experiment (Table 1).

[36] The first set of 3 sensitivity tests concerned the time steps used in our modeling work. The increase of the model integration time step from 5 to 15 min slightly degraded the representation of the mixed layer depth (not shown), but did not significantly affect the averaged rates of biological net DMS production or the mean surface DMS flux ($\leq$2.7%; Table 1). The reduction of the inversion time step from 1 h to 5 min (equal to the model integration time step) or conversely its expansion to 3 h had also only a slight impact on the results ($\leq$5%; Table 1).

[37] The second set of 5 sensitivity tests addressed the physical part of the model. First, we tested its sensitivity to the turbulence scheme used by GOTM. Instead of the k-ε turbulence closure scheme, we used the Mellor-Yamada (MY) 2.5 turbulence closure scheme [*Burchard and Petersen*, 1999]. The simulated changes of the turbulent mixed layer were relatively small (<5% on average over the study). The MY scheme generated a slightly shallower mixed layer (not shown), but reproduced the same temporal pattern. Secondly, we tested its sensitivity to the T/S restoring time constant which was set to 6 h (instead of 24 h) both at the surface and in the water column, or to 5 d in the water mass and 24 h at the surface. An additional test was performed for the "out patch" inversion by using the T/S observations from the "out patch" stations instead of the "in patch" data. None of these changes significantly affected the averaged rates of biological net DMS productions or the mean surface DMS flux ($\leq$5.2%; Table 1). On the other hand, the removal of the dilution effect in an "in patch" sensitivity inversion affected the averaged rates of biological net DMS production, especially during stage 2 (by −18.9%) when the difference of DMS concentrations between inside and outside the patch was the highest. Without the dilution effect, no DMS was imported from outside the patch during stage 2 and the DMS consumption was reduced. However, this compensation had no significant effect on the surface DMS flux ($\sim$0.1%).

[38] In the third set of 3 sensitivity tests, we changed the other components of the DMS budget. First, two different parameterizations were used to calculate the surface DMS flux [*Liss and Merlivat*, 1986; *Wanninkhof*, 1992]. The mean DMS fluxes, both outside and inside the patch, were decreased by $\sim$29% in the first case [*Liss and Merlivat*, 1986] and increased by $\sim$25% in the second [*Wanninkhof*, 1992] compared to the reference inversions (Table 1). Second, the photodegradation DMS sink was simply removed from the budget equation (1), resulting in a $\sim$41% relative increase in biological net DMS production during stage 2 outside the patch. These tests altered the averaged rates of biological net DMS production during the two stages, both inside and outside the patch (Table 1), but not the temporal evolutions of the reconstructions (not shown). The relative differences between stages 1 and 2 and between inside and outside the patch were not significantly affected. However, the large relative changes from the reference inversions reflect a higher sensitivity to the ventilation and photodegradation parameterization, especially when the reconstructed biological net DMS production was low (e.g., outside the patch during stage 2).

[39] These sensitivity tests indicate that our reconstructed biological net DMS productions were not dependent (sensitivity less than 5%) on basic technical choices in the model setup (model integration and inversion time steps, T/S restoring, turbulence scheme). On the other hand, they also show that the imprecisions inherent in the parameterizations used (patch dilution effect, surface ventilation, photodegradation) can affect the absolute values of the reconstructed biological net DMS production but not the

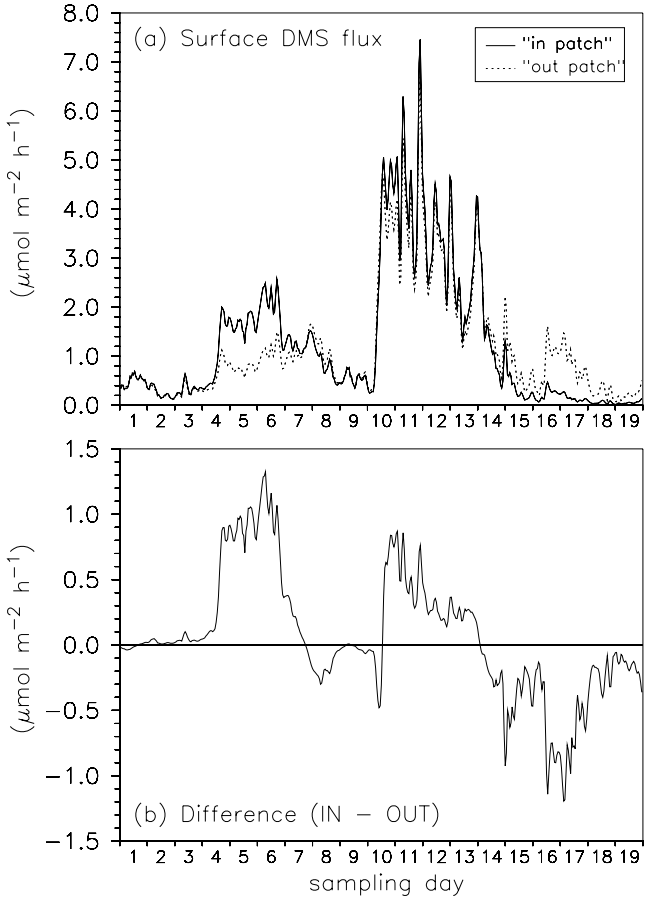

Figure 7. Time evolution (3 h running mean) of (a) the sea-air DMS flux (μmol m^{-2} h^{-1}) inside (solid line) and outside (dotted line) the Fe-enriched patch and (b) the difference of DMS flux (μmol m^{-2} h^{-1}) between the inside and the outside areas of the patch.

time evolution patterns of the reconstructed biological net DMS production and more specifically, the differences found between the two stages of the experiment and between inside and outside the patch. This persistence in the reconstructed variations confirms the robustness of our inverse modeling results.

5. Discussion

5.1. Impact of Iron on Processes Regulating the DMS Budget in the Mixed Layer

[40] On the basis of our integrated DMS budget in the mixed layer, we evaluated the relative importance of the different processes responsible for the DMS distribution in the TML inside and outside the Fe-enriched patch and assess the impact of iron on these processes.

[41] DMS photodegradation was not the dominant process (generally less than 0.1 nmol L^{-1} h^{-1}) either outside or inside the patch (Figure 6a). However, its impact on the mixed layer DMS budget was more important (of similar magnitude to the ventilation) during periods of shallow mixed layer depth, such as during day 9. At the end of the experiment, photodegradation became slightly lower inside than outside the patch because of the lower levels of DMS and the decrease in NO_3^- concentration resulting from the iron-induced diatom bloom [*Bouillon and Miller*, 2004].

[42] The vertical entrainment of DMS resulted from the mixing between the mixed layer and waters below due to vertical diffusion and advection and especially due to the changes in the TML depth. Entrainment fluxes were generally low (<0.1 nmol L^{-1} h^{-1}), with a single peak on day 10 when the TML rapidly deepening (Figure 6b). This rapid entrainment of DMS to the surface resulted from the previous accumulation of DMS at depth. During the shoaling event that preceded the deepening, lower photodegradation at depth and the absence of ventilation resulted in the buildup of a DMS pool trapped in the subsurface layer. Inside the patch, the influence of iron was effective down to the tracer layer depth that followed, since day 4, the seasonal pycnocline located at around 30 m on average. During the temporary shoaling event, the biological net DMS production below the TML was higher inside the patch than outside (not shown), contributing to a DMS concentration maximum in subsurface water that was ~1.5 fold larger inside the patch than outside. Accordingly, the DMS redistribution in the surface mixed layer was larger inside the patch than outside once vertical entrainment occurred. The peak in the surface DMS concentration maximum observed on day 11 both inside and outside the patch resulted from this physical redistribution process.

[43] Among the physical mechanisms, the sea-to-air surface ventilation was the most important, except on day 10 when vertical entrainment of DMS was playing a dominant role, even exceeding the role of biological processes. The amount of DMS ventilated to the atmosphere mainly depends on the surface wind speed and the concentration of DMS in the upper ocean mixed layer [*Kettle and Andreae*, 2000]. Although the impact of DMS surface ventilation on the mixed layer DMS budget was mainly driven by the wind speed, the differences in DMS flux between inside and outside the patch also reflected the differences in surface DMS concentrations (Figure 7). Coinciding with high surface DMS concentrations and high wind speed, the DMS flux was maximal between days 11 and 14. This enhanced DMS lost contributed to the negative net DMS balance in the TML (Figure 6e) that resulted in the reduction of DMS in the mixed layer. The surface DMS flux inside the patch was enhanced by +6.5 μmol m^{-2} d^{-1} (+23%) during stage 1 and reduced by −5.5 μmol m^{-2} d^{-1} (−18.3%) during stage 2 compared to the mean fluxes outside the patch. When averaged over the whole experiment, the total amount of DMS ventilated to the atmosphere from the Fe-enriched patch was almost the same (~+5%; Table 1) as from the surrounding HNLC waters. Given the uncertainties associated with these measurements (~10% for DMS determination only), this difference in the mean DMS flux is probably not significant. Furthermore, if we assume that the depletion of surface DMS inside the patch is maintained over several days, the reduction in DMS ventilation from the Fe-enriched patch will be maintained also, and the time-integrated impact on the averaged DMS flux should become negative. In any case, our results indicate that the iron enrichment in the subarctic Northeast Pacific did not create favorable conditions that could mitigate climate warming through an increase in marine sulfate aerosols.

[44] As previously mentioned, our modeling results show that the influence of variations in wind speed on vertical mixing and sea-to-air flux cannot alone explain the temporal distribution of DMS both outside and inside the patch during SERIES. The DMS budget in the upper mixed layer was largely determined by changes in biological net DMS production. Although there are strong similarities in the variability in biological net DMS productions reconstructed inside and outside the patch during the two stages, the iron enrichment had two impacts on biological processes.

[45] The first effect was to increase the mean biological net DMS production relatively to outside the patch during stage 1 (days 1–11), in relation with the development of a DMSP-rich nanophytoplankton bloom, but less than expected with respect to the DMSP produced. The stimulation of biological net DMS production was principally apparent during days 4 and 5, leading to the increases in DMS concentration in the TML and in surface DMS flux. Unfortunately, this stimulation effect is poorly constrained because of the absence of DMS measurements outside the patch during days 5 and 7, which limits the possible interpretation of the differences between inside and outside the patch during this period. Furthermore, the variability in biological net DMS production was also increased inside the patch during stage 1, suggesting a more complex response of the microbial system than a direct relationship to the size of the DMSP pool.

[46] The second effect, more important and better constrained, consisted in a reduction in biological net DMS production as compared to outside the patch during the full development of the diatom bloom, when the DMSPp concentrations inside the patch was similar to those outside. Our results clearly show that during stage 2, the iron enrichment exacerbated a natural decrease in biological net DMS production that was already taking place in the study area. During the last week of the experiment (days 12–19), the biological processes represented a sink for DMS inside the patch and DMS concentrations fell to levels largely below those observed outside the patch.

[47] Over the first 19 days of SERIES, the iron enrichment induced an overall reduction of the DMS production efficiency by the microbial system. It is also interesting to note the increase in the variability of the biological net DMS production inside the patch during the experiment, reflecting rapid destabilization of the microbial system probably due to sudden infusions of dissolved organic material.

5.2. Interpretation of the Variations in Reconstructed Biological Net DMS Production Outside the Fe-Enriched Patch

[48] Outside the Fe-enriched patch, the highest biological net DMS productions were reconstructed on days 6–8 during a period characterized by high surface solar radiation and decreasing wind speed (Figure 5). These environmental conditions resulted in higher underwater light exposure for phytoplankton cells and bacteria in the surface mixed layer. In contrast, wind speed and vertical mixing were enhanced after day 10, while surface solar radiation was reduced. High radiation (specifically UV light) has been linked to increased DMSP content in *Emiliana huxleyi* [*Slezak and Herndl*, 2003], increased DMS production [*Sunda et al.*, 2002; *Toole and Siegel*, 2004], and decreased bacterial DMS consumption [*Slezak et al.*, 2001]. The variations of biological net DMS production may represent a rapid response of the microbial system to alterations in the radiative conditions in the TML [*Simó and Pedrós-Alió*, 1999].

[49] Although the broad temporal features of the reconstructed biological net DMS production can be related to surface irradiance and wind speed, there are certainly other variations that do not support this interpretation. The daily surface radiation was high during the first 3 sampling days, yet our reconstructions show no increase in biological net DMS production during this period. Both surface DMSPp and DMSPd concentrations were higher on day 1 than during all the following observations, suggesting that the sampling began during a period of change in DMS(P) dynamics. On day 14, the increase of biological net DMS production may be linked to a temporary increase of phytoplankton production as reflected by the small increase in chlorophyll *a* concentration (Figure 1a). One can also discern a recovery of biological net DMS productions toward positive values as the mixed layer gradually shallows toward the end of the experiment. In spite of these transients operating at different timescales that complicate the interpretation, our results suggest that a combination of high irradiance and low wind-driven turbulence led to increased biological net DMS production outside the patch during stage 1. In agreement with the previous studies of *Simó and Pedrós-Alió* [1999] and *Toole and Siegel* [2004], our results also highlight the complexity in the relationship on short timescales between net DMS production and environmental conditions.

[50] Variations in biological net DMS production may result from variations in algal and/or bacterial DMS production or from variations in bacterial DMS consumption [*Simó*, 2001]. Our modeling results cannot discriminate between production and loss processes that underpin these variations in biological net DMS production. Our interpretation of the DMS dynamics is further limited by the weak temporal resolution of the DMSP measurements in the untreated waters (5 stations). It is nevertheless interesting to note that the lowest surface DMSPd concentrations (days 6 and 19) were associated with high reconstructed biological net DMS productions, and the highest DMSPd concentrations (days 11 and 16, and even day 1) were associated with low productions, suggesting possible variations in the transformation efficiency from DMSPd to DMS. The dynamics of the oceanic microbial food web and the production of DMSPd and ultimately DMS, in particular via the grazing pathway [*Dacey and Wakeman*, 1986], could also have been altered by the environmental changes (radiation, vertical mixing). The biological mechanisms that underpin these variations needs to be studied with a biogeochemical model including not only the complete DMS(P) cycling [*Le Clainche et al.*, 2004] but also the impact of environmental conditions on microbial transformations on DMS(P).

5.3. Interpretation of the Variations in Reconstructed Biological Net DMS Production Inside the Fe-Enriched Patch

[51] The rapid increase of the reconstructed biological net DMS production on day 4 (Figure 6d) coincided with the rapid increase in the abundance of DMSP-rich prymnesio-

phytes in the iron-enriched patch, and the resulting increase in DMSPp (Figure 1b). However, the production decreased to zero later on (days 5 to 7) while the DMSPp was still elevated. The concomitant increase of DMSPd (Figure 1c) suggests that the dynamics of the microbial system changed during the development of the nanophytoplankton bloom, resulting in a reduction of the bacterial DMSPd consumption and DMS yield (the efficiency at which DMSP consumed by bacteria is converted to DMS). At the same time, the biological net DMS production was maximal outside the patch, suggesting that the DMS(P) dynamics was driven by the iron enrichment inside the patch. These rapid variations in biological net DMS production inside the patch contributed to counterbalance the differences in DMS concentrations between inside and outside the patch. As noted before, this apparent alteration of the biological net DMS production during this period (days 4 to 7) was poorly constrained by our ''out patch'' measurements and need further confirmation.

[52] Between days 10 and 13, the crash of the nanophytoplankton bloom and the rapid decrease in DMSPp concentrations (Figure 1b) were paralleled by a rapid decrease in the reconstructed biological net DMS production, which became negative after day 12 (Figure 6d). The shift in the phytoplankton assemblage toward weak DMSP producers (diatoms) is not sufficient to explain such a rapid decline in DMS production, since similar low DMSPp concentrations outside the patch were associated with higher biological net DMS production rates during that period (Figures 1b and 6d). Bacteria can use DMSP either as a carbon source, via a cleavage pathway that produces acrylate and DMS, or as a carbon and sulfur source, via a demethylation pathway that does not produce DMS [*Kiene et al.*, 2000; *Simó*, 2004]. During days 10–13, the DMSPd concentration showed no increase, suggesting that the DMSP was consumed by bacteria and used predominantly as a sulfur source [*Kiene et al.*, 2000] with very low DMS yield. The very high bacterial production and DMSPd consumption rates measured during this period support this interpretation (A. Merzouk et al., DMSP and DMS dynamics during a mesoscale iron fertilization experiment in the northeast Pacific. part II. Biological cycling, submitted to *Deep-Sea Research, Part II*, 2005; M. S. Hale et al., Microbial response to a mesoscale iron enrichment in the NE subarctic Pacific: Heterorophic bacterial processes, submitted to *Deep-Sea Research, Part II*, 2005). Bacterial production remained high during the following diatom bloom (days 12–17), keeping the net biological DMS production low. These results suggest that changes in bacterial DMSP metabolism were responsible for the decrease in biological DMS net production calculated from our inverse reconstruction.

6. Summary and Conclusions

[53] We used an inverse modeling approach to reconstruct biological net DMS production by combining the available DMS observations with a simulation of the physical (turbulent diffusion, ventilation) and photochemical (photodegradation) processes that affect DMS concentrations. Basically, we assumed that physical and photochemical processes can be quantified using known approaches and measurements and that the differences between the DMS concentrations simulated using only physicochemical processes and the concentrations observed can be attributed to biological processes. Our extensive sensitivity analyses indicate that our reconstructions of biological net fluxes are robust to variations in the parameterizations of the physical and photochemical processes. This modeling study is the first to develop an integrated dynamical budget of DMS during a large-scale iron enrichment experiment both inside and outside the Fe-enriched patch. We believe that such an approach can be applied to other sets of DMS measurements, such as Lagrangian studies, and that reconstructed biological net DMS productions can be very useful in the development of more complete mechanistic models of DMS(P) cycling. This is also a powerful tool to compare DMS dynamics in different large-scale iron enrichment experiments.

[54] This study highlights the importance of short-term variability in mixing conditions on DMS dynamics. The succession between calm and turbulent periods can lead to sharp peak in DMS flux to the atmosphere resulting from vertical entrainment of DMS trapped below the surface turbulent mixed layer. This confirms that a modeling study of surface oceanic DMS pool on short periods should be based on an accurate physical upper ocean model to capture the dynamics of the surface mixed layer and the effects of rapid physical perturbations. The impact of the sequence of stabilization-destabilization events on mean DMS flux over longer timescales need to be determined.

[55] Our results also revealed the strong short-term (<day) variability in biological net DMS production at the reference station (outside the Fe-enriched patch) over a 3-week period when chlorophyll *a* and particulate DMSP (indicators of system productivity) were stable. It appears that variations in biological net DMS production can be best related to changes in bacterial DMS yield induced by environmental conditions (surface radiation and turbulence). The role of physical forcing in DMS(P) cycling, particularly the effect of light on biological DMSP production and utilization, still needs further investigation in both experimental and modeling studies. At the very least, this work argues that the control ''out patch'' station should be sampled at high frequency, like the ''in patch'' station during future experiments.

[56] Similarly, the effect of iron enrichment on biological net DMS production was complex and was linked not only to iron induced changes in phytoplankton biomass and taxonomic composition (dominance of nanophytoplanktons versus diatoms), but also to rapid changes in the bacterial DMS(P) dynamics. After the initial increase in nanophytoplankton abundance and DMS(P), the iron enrichment reduced the DMS production efficiency of the microbial system, leading to biological net DMS consumption during the diatom bloom. Previous studies on the impact of iron on DMS production in HNLC regions have mostly focused on autotrophic organisms. Our results show that heterotrophic organisms must be considered as well, and their role carefully parameterize in mechanistic model of the DMS(P) cycling.

[57] **Acknowledgments.** This work is a contribution of the Canadian-SOLAS Network (Surface Ocean-Lower Atmosphere Study) funded by the Natural Sciences and Engineering Research Council of Canada (NSERC), the Canadian Foundation for Climate and Atmospheric Sciences (CFCAS), the Department of Fisheries and Oceans Canada, and the Department of

Environment Canada. The authors wish to address special thanks to all the Canadian SOLAS members who participated in the SERIES mission and especially to the providers of the data who were indispensable for this modeling study: Frank Whitney and Marie Robert for the T/S data from the ship *CCGS John P. Tully*, Atsushi Tsuda for the T/S data from the Japanese ship *Kaiyo Maru*, Nelson Sherry for the T/S data from the ship *B/O El Puma*, and Lisa Phinney for the onboard meteorological data. This work would have not been possible without the professional support from the captains and crew members of the *B/O El Puma*, *CCGS John P. Tully*, and *Kaiyo Maru*. The manuscript greatly benefited from comments by Hein De Baar and one anonymous reviewer. We also thank the core team of ocean modelers who develop and support GOTM (www.gotm.net). The graphics were created with the Ferret program. Ferret is a product of NOAA's Pacific Marine Environmental Laboratory (www.ferret.noaa.gov).

References

Andreae, M. O., and P. J. Crutzen (1997), Atmospheric aerosols: Biogeochemical sources and role in the atmospheric chemistry, *Science*, *276*, 1052–1058.

Archer, S. D., F. J. Gilbert, J. I. Allen, J. Blackford, and P. D. Nightingale (2004), Modelling of the seasonal patterns of dimethylsulfide production and fate during 1989 at a site in the North Sea, *Can. J. Fish. Aquat. Sci.*, *61*(5), 765–787.

Baliño, B. M., M. J. R. Fasham, and M. C. Bowles (2001), Ocean biogeochemistry and global change, JGOFS, *IGBP Sci. Ser. 2*, 32 pp., Int. Geosphere Biosphere Programme, Stockholm.

Barnard, W. R., M. O. Andreae, W. E. Watkins, H. Bingemer, and H.-W. Georgii (1982), The flux of dimethylsulfide from the oceans to the atmosphere, *J. Geophys. Res.*, *87*(C11), 8787–8793.

Bates, T. S., B. K. Lamb, A. Guenther, J. Dignon, and R. E. Stoiber (1992), Sulfur emissions to the atmosphere from natural sources, *J. Atmos. Chem.*, *14*, 315–337.

Bopp, L., O. Aumont, S. Belviso, and P. Monfray (2003), Potential impact of climate change on marine dimethylsulfide emissions, *Tellus, Ser. B*, *55*(1), 11–22.

Bouillon, R.-C., and W. L. Miller (2004), Determination of apparent quantum yield spectra of DMS photodegradation in an in-situ iron-induced northeast Pacific Ocean bloom, *Geophys. Res. Lett.*, *31*, L06310, doi:10.1029/2004GL019536.

Boyd, P. W., et al. (2004), The decline and fate of an iron-induced subarctic phytoplankton bloom, *Nature*, *428*, 549–553.

Brainerd, K. E., and M. C. Gregg (1995), Surface mixed and mixing layer depths, *Deep Sea Res., Part I*, *42*(9), 1527–1543.

Burchard, H., and O. Petersen (1999), Models of turbulence in the marine environment—A comparative study of two-equation turbulence models, *J. Mar. Syst.*, *21*, 29–53.

Burchard, H., K. Bolding, and M. R. Villarreal (1999), GOTM—A general ocean turbulence model. Theory, applications and test cases, *Tech. Rep. EUR 18745*, 103 pp., Eur. Comm., Brusssels.

Charlson, R. J., J. E. Lovelock, M. O. Andreae, and S. G. Warren (1987), Oceanic phytoplankon, atmospheric sulfur, cloud albedo and climate, *Nature*, *326*, 655–661.

Chisholm, S. W., and F. M. M. Morel (Eds.) (1991), What controls phytoplankton production in nutrient-rich areas of the open sea?, *Limnol. Oceanogr.*, *36*.

Clarke, A. D., J. L. Varmer, F. Eisele, R. L. Maudlin, D. Tanner, and M. Litchy (1998), Particle nucleation in the tropical boundary layer and its coupling to marine sulfur sources, *Science*, *282*, 89–92.

Cummins, P. F., and G. S. Lagerloef (2002), Low frequency pycnocline depth variability at station P in the northeast Pacific, *J. Phys. Oceanogr.*, *32*(11), 3207–3215.

Dacey, J. W. H., and S. G. Wakeman (1986), Oceanic DMS: Production during zooplankton grazing on phytoplankton, *Science*, *233*, 1314–1316.

de Baar, H. J. W., et al. (2005), Synthesis of iron fertilization experiments: From the Iron Age in the Age of Enlightenment, *J. Geophys. Res.*, *110*, C09S16, doi:10.1029/2004JC002601.

Gabric, A. J., R. Cropp, T. Hirst, and H. Marchant (2003), The sensitivity of dimethyl sulfide production to simulated climate change in the eastern Antarctic Southern Ocean, *Tellus, Ser. B*, *55*(5), 966–981.

Kalnay, E., et al. (1996), The NCEP/NCAR 40-year reanalysis project, *Bull. Am. Meteorol. Soc.*, *77*(3), 437–472.

Kantha, L. H., and C. A. Clayson (1994), An improved mixed layer model for geophysical applications, *J. Geophys. Res.*, *99*(C12), 25,235–25,266.

Keller, M. D. (1989), Dimethylsulfide production and marine phytoplankton: The importance of species composition and cell size, *Biol. Oceanogr.*, *6*(5–6), 375–382.

Kettle, A. J., and M. O. Andreae (2000), Flux of dimethylsulfide from the oceans: A comparison of updated data sets and flux models, *J. Geophys. Res.*, *105*(D22), 26,793–26,808.

Kettle, A. J., et al. (1999), A global database of sea surface dimethylsulfide (DMS) measurements and a procedure to predict sea surface DMS as a function of latitude, longitude, and month, *Global Biogeochem. Cycles*, *13*(2), 399–444.

Kiene, R. P., and T. S. Bates (1990), Biological removal of dimethyl sulfide from sea water, *Nature*, *345*, 702–705.

Kiene, R. P., P. T. Visscher, M. D. Keller, and G. O. Kirst (Eds.) (1996), *Biological and Environmental Chemistry of DMSP and Related Sulfonium Compounds*, Springer, New York.

Kiene, R. P., L. J. Linn, and J. A. Bruton (2000), New and important roles for DMSP in marine microbial communities, *J. Sea Res.*, *43*, 209–224.

Large, W. G., J. C. McWilliams, and S. C. Doney (1994), Oceanic vertical mixing: A review and a model with non-local boundary layer parameterization, *Rev. Geophys.*, *32*(4), 363–403.

Lawrence, M. G. (2002), Side effects of oceanic iron fertilization, *Science*, *297*, 1993.

Le Clainche, Y., M. Levasseur, A. Vézina, J. W. H. Dacey, and F. J. Saucier (1994), Behaviour of the ocean DMS (P) pools in the Sargasso Sea viewed in a coupled physical-biogeochemical ocean model, *Can. J. Fish. Aquat. Sci.*, *61*(5), 788–803.

Liss, P. S., and L. Merlivat (1986), Air-sea gas exchange rates: Introduction and synthesis, in *The Role of Air-Sea Exchange in Geochemical Cycle*, edited by Buat-Ménart, P., , pp. 113–129, Springer, New York.

Liss, P. S., G. Malin, S. M. Turner, and P. M. Holligam (1994), Dimethyl sulfide and phaeocystis—A review, *J. Mar. Syst.*, *5*, 41–53.

Malin, G., and G. O. Kirst (1997), Algal production of dimethylsulfide and its atmospheric role, *J. Phycol.*, *33*, 889–896.

Martin, J. H., and S. E. Fitzwater (1988), Iron deficiency limits phytoplankton growth in the north-east Pacific subarctic, *Nature*, *331*, 341–343.

Nightingale, P. D., G. Malin, C. S. Law, A. J. Watson, P. S. Liss, M. I. Liddicoat, J. Boutin, and R. C. Upstill-Goddard (2000), In situ evaluation of air-sea gas exchange parameterizations using novel conservative and volatile tracers, *Global Biogeochem. Cycles*, *14*(1), 373–387.

Parker, R. L. (Ed.) (1994), *Geophysical Inverse Theory*, 386 pp., Princeton Univ. Press, Princeton, N. J.

Press, W. H., B. P. Flannery, S. A. Teukolsky, and W. T. Vetterling (Eds.) (1986), *Numerical Recipes: The Art of Scientific Computing*, 818 pp., Cambridge Univ. Press, New York.

Saltzman, E. S., D. B. King, K. Holmen, and C. Leck (1993), Experimental determination of the diffusion coefficient of dimethylsulfide in water, *J. Geophys. Res.*, *98*(C9), 16,481–16,486.

Scarratt, M. G., M. Levasseur, S. Michaud, G. Cantin, M. Gosselin, and S. J. de Mora (2002), Influence of phytoplankton taxonomic profile on the distribution of dimethylsulfide and dimethylsulfoniopropionate in the northwest Atlantic, *Mar. Ecol. Prog. Ser.*, *244*, 49–61.

Simó, R. (2001), Production of atmospheric sulfur by oceanic plankton: Biogeochemical, ecological and evolutionary links, *Trends Ecol. Evol.*, *16*(6), 287–294.

Simó, R. (2004), From cells to globe: Approaching the dynamics of DMS (P) in the ocean at multiple scales, *Can. J. Fish. Aquat. Sci.*, *61*(5), 673–684.

Simó, R., and C. Pedrós-Alió (1999), Short-term variability in the open ocean cycle of dimethylsulfide, *Global Biogeochem. Cycles*, *13*(4), 1173–1181.

Slezak, D., and G. J. Herndl (2003), Effects of ultraviolet and visible radiation on the cellular concentrations of dimethylsulfoniopropionate (DMSP) in *Emiliana* huxleyi (strain L), *Mar. Ecol. Prog. Ser.*, *246*, 61–71.

Slezak, D., A. Brugger, and G. J. Herndl (2001), Impact of solar radiation on the biological removal of dimethylsulfoniopropionate and dimethylsulfide in marine surface waters, *Aquat. Microb. Ecol. Proc. Conf.*, *25*, 87–97.

Sunda, W., D. J. Kieber, R. P. Kiene, and S. Huntsman (2002), An antioxidant function for DMSP and DMS in marine algae, *Nature*, *418*, 317–320.

Toole, D. A., and D. A. Siegel (2004), Light-driven cycling of dimethylsulfide (DMS) in the Sargasso Sea: Closing the loop, *Geophys. Res. Lett.*, *31*, L09308, doi:10.1029/2004GL019581.

Toole, D. A., D. J. Kieber, R. P. Kiene, D. A. Siegel, and N. B. Nelson (2003), Photolysis and the dimethylsulfide (DMS) summer paradox in the Sargasso Sea, *Limnol. Oceanogr.*, *48*, 1088–1100.

Turner, S. M., P. D. Nightingale, L. J. Spokes, M. I. Liddicoat, and P. S. Liss (1996), Increased dimethyl sulphide concentrations in sea water from in situ iron enrichment, *Nature*, *383*, 513–516.

Turner, S. M., M. J. Harvey, C. S. Law, P. D. Nightingale, and P. S. Liss (2004), Iron-induced changes in oceanic sulfur biogeochemistry, *Geophys. Res. Lett.*, *31*, L14307, doi:10.1029/2004GL020296.

Vézina, A. F. (2004), Ecosystem modelling of the cycling of marine dimethylsulfide: A review of current approaches and of the potential for extrapolation to global scales, *Can. J. Fish. Aquat. Sci.*, *61*(5), 845–856.

Wanninkhof, R. (1992), Relationship between wind speed and gas exchange over the ocean, *J. Geophys. Res.*, *97*(C5), 7373–7382.
Watson, A. J., and P. S. Liss (1998), Marine biological controls on climate via the carbon and the sulphur geochemical cycles, *Philos. Trans. R. Soc. London, Ser. B*, *353*, 41–51.
Wong, C.-S., S. E. Wong, W. A. Richardson, G. E. Smith, M. D. Arychuk, and J. S. Page (2005), Temporal and spatial distribution of dimethylsulfide in the subarctic northeast Pacific Ocean: A high-nutrient-low-chlorophyll region, *Tellus, Ser. B*, *57*(4), 317–331.

R.-C. Bouillon, Department of Chemistry and Biochemistry, University of North Carolina at Wilmington, Wilmington, NC 28403, USA.
P. W. Boyd, Centre for Chemical and Physical Oceanography, NIWA and Department of Chemistry, University of Otago, PO Box 56, Dunedin, 9001, New Zealand.
P. J. Harrison, Atmospheric, Marine and Coastal Environment Program, Hong Kong University of Science and Technology, Clear Water Bay, Hong Kong, China.
C. S. Law, National Institute of Water and Atmospheric Research, 301 Evans Bay Parade, Greta Point, PO Box 14-901, Wellington, 6003, New Zealand.
Y. Le Clainche, M. Levasseur, and A. Merzouk, Département de Biologie (Québec-Océan), Université Laval, Québec, QC, Canada G1K 7P4. (yvonnick.leclainche@giroq.ulaval.ca)
S. Michaud and M. Scarratt, Maurice Lamontagne Institute, Fisheries and Oceans Canada, PO Box 1000, 850 Route de la Mer, Mont-Joli, QC, Canada G5H 3Z4.
W. L. Miller, Department of Marine Sciences, University of Georgia, Marine Sciences Bldg., Athens, GA 30602, USA.
R. B. Rivkin, Ocean Sciences Centre, Memorial University of Newfoundland, St. John's, NF, Canada A1C 5S7.
F. J. Saucier, Institut des Sciences de la Mer de Rimouski, Université du Québec à Rimouski, PO Box 3300, 310 Allée des Ursulines, Rimouski, QC, Canada G5L 3A1.
A. Vézina, Bedford Institute of Oceanography, Fisheries and Oceans Canada, PO Box 1006, Dartmouth, NS, Canada B2Y 4A2.
C. S. Wong, Institute of Ocean Sciences, Fisheries and Oceans Canada, PO Box 6000, Sidney, BC, Canada V8L 4B2.